Received: 31 May 2024 | Revised: 26 September 2024 | Accepted: 28 September 2024

DOI: 10.1002/zamm.202400554

ORIGINAL PAPER

Mathematical thermo-mechanical analysis on flame-solid interaction: Steady laminar stagnation flow flame stabilized at a plane wall coupled with thermo-elasticity model

Chunkan Yu[1] | **Mohammad Mahdi Malayeri**[1] | **Thomas Böhlke**[2] | **Zheng Chen**[3] | **Felipe Minuzzi**[4]

[1]Institute of Technical Thermodynamics, Karlsruhe Institute of Technology (KIT), Karlsruhe, Baden-Württemberg, Germany

[2]Institute of Engineering Mechanics, Karlsruhe Institute of Technology (KIT), Karlsruhe, Baden-Württemberg, Germany

[3]HEDPS, SKLTCS, CAPT, College of Engineering, Peking University, Beijing, China

[4]Department of Mathematics, Federal University of Santa Maria, Santa Maria, Brazil

Correspondence
Chunkan Yu, Institute of Technical Thermodynamics, Karlsruhe Institute of Technology (KIT), Karlsruhe, Baden-Württemberg, Germany.
Email: chunkan.yu@kit.edu

Funding information
DFG, Grant/Award Number: 523879740; NSFC, Grant/Award Number: 52176096;

A laminar stagnation flow flame stabilized at a plane wall is theoretically analyzed, coupled with a thermo-elasticity model in the wall. Mathematical models for both the flame and the wall will be proposed, and corresponding analytical solutions based on their dimensionless forms will be obtained. The mathematical analysis of this flame-solid interaction primarily focuses on the effect of the flame on combustion-induced thermo-mechanical stresses and the influence of wall material on flame properties such as flame temperature and stability against extinction. A sensitivity analysis is further performed to examine how thermo-mechanical stress inside the wall is affected by changes in other combustion conditions (e.g., mixture composition, flame stretch rate). This study offers valuable insights into understanding the interaction between flames and solids, a relationship crucial in engineering applications such as the interaction between combustion processes and blades within gas turbine machinery.

1 | INTRODUCTION

Combustion processes are important to numerous engineering applications, ranging from power generation to transportation. The interaction between combustion process and solid introduces complex phenomena that significantly impact combustion efficiency and environmental considerations, and the selection of materials significantly affect the combustion efficiency and properties. For example, the combustion chamber head made from aluminium alloy leads to a higher unburnt hydrocarbon (HC) formation compared to cast iron [1, 2].

On the other hand, the combustion process has a noticeable influence on material and mechanical properties. Optimizing the combustion process is essential to avoid thermal failure, as flame temperatures are typically high (above 1800 K in most cases) [3]. Moreover, the elevated flame temperature may induce significant strain of solid materials, potentially

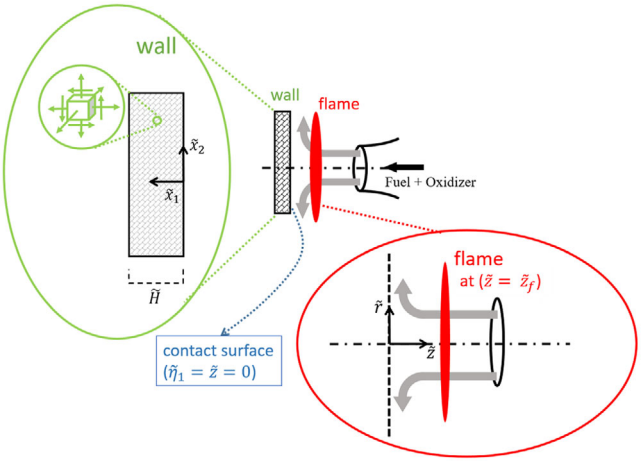

FIGURE 1 Schematic illustration of studied flame-solid interaction.

leading to elasto-plastic strain. This can result in phenomena such as hydrogen embrittlement, shortening the materials lifetime [4, 5]. Additionally, as demonstrated in material failure analysis [6–8], combustion instabilities such as noise, vibrations, and thermo-acoustic phenomena may cause unsteady wall displacement of combustion chamber components, thereby increasing the risk of material failure.

While solid mechanics and combustion processes have been extensively modeled theoretically and numerically separately, coupled models for both processes are less reported. A stagnation flow flame stabilized at a plane wall represents one of the simplest configurations in which the combustion process interacts with solid materials. However, in many cases, the wall temperature is commonly set to be fixed or adiabatic, with the primary focus on investigating the influence of wall temperature on flame properties [9, 10]. Another commonly studied configuration is flame-wall interaction, which describes the quenching process for a premixed flame propagating towards or along a cold wall [11–14]. A thermal formulation based on the first law of thermodynamics is often derived, describing the relationship between quenching distance and heat flux, while also considering the effects of pressure and mixture composition [12].

Recently, the flame-solid interaction has been further modeled to include the effect of the combustion process on strain [15] and thermo-mechanical stress [16, 17]. In these studies, computational fluid dynamics (CFD) methods are used to simulate the combustion process simultaneously with the structural governing equations for solid mechanics, allowing for the prediction of strain and thermo-mechanical stress inside the material. Such coupled models are useful for the design and prognosis of combustion engineering applications.

The present work aims to provide a general theoretical description of a stagnation flow flame stabilized at a plane wall coupled with a thermo-elasticity model to assess: i) the effect of the combustion process on thermo-mechanical loading inside the material, and ii) the influence of material selection with different thermal resistance on flame properties (e.g., flame temperature, flame position, laminar burning velocity, and extinction limit). In the next section, theoretical models and analytical solutions are presented. Then in Section 3, the flame-solid interaction is examined. Finally, the conclusions are given in Section 4. Based on the present mathematical analysis, a general correlation between the combustion process and thermo-mechanical stresses inside the wall is derived for the first time. This model can be used to assess the effects of stretch rate and Lewis number on premixed counterflow flame structure and combustion-induced thermo-mechanical stresses.

Notation. For the thermo-elastic continuum mechanical model in the plane wall, vectors and tensors are written in index notation using the Einstein Summation convention (e.g., u_i for the displacement vector and σ_{ij} for stress tensor). In the corresponding matrix notation the variables are double underlined.

2 | MATHEMATICAL MODEL AND ANALYTICAL SOLUTION

In this study, we examine an adiabatic premixed stagnation flow flame stabilized at a plane wall, as illustrated in Figure 1. The fuel and oxidizer are fully homogeneous and premixed, exiting the burner nozzle. If the flow velocity remains below a

critical threshold, ensuring flame extinction does not occur, a stable burning flame impinging normal to a plane surface is observed. The high flame temperature (approximately 1800 K or higher [18–20]) leads to an increased contact temperature at the wall surface, inducing thermal expansion and thermo-mechanical stresses within the wall.

Despite its straightforward configuration, this setup proves a valuable possibility in understanding the interaction between the flame and solid surfaces, a relationship crucial in engineering applications such as the interaction between the combustion process and blades within gas turbine machinery. In the subsequent sections, we will introduce the model for the laminar stagnation flow flame, the model for the plane wall, and their respective analytical solutions. Assumptions and simplifications made for each model will be introduced as well. Furthermore, it is essential to note that all symbols and variables without a tilde are non-dimensional, and vice versa.

2.1 | Model for laminar stagnation flow flame at a plane wall

For the model of a laminar stagnation flow flame stabilized at a plane wall, we treat it as a one-dimensional adiabatic premixed laminar flame, where all thermo-kinetic quantities are solely dependent on the $\tilde{z}$-coordinate (cf. Figure 1). These quantities encompass the temperature $\tilde{T}_g = \tilde{T}_g(\tilde{z})$ and fuel mass fraction $\tilde{Y}_F = \tilde{Y}_F(\tilde{z})$. To account for the influence of flow velocity on flame properties, the flow velocity field remains two-dimensional. Following the widely-used assumption for the asymptotic analysis of strained premixed flames [21–23], we assume a potential flow without considering the boundary layer on the wall surface to define the flow velocity as:

$$\underline{\tilde{v}} = \begin{pmatrix} \tilde{v}_z \\ \tilde{v}_r \end{pmatrix} = \begin{pmatrix} -\tilde{k}\tilde{z} \\ \tilde{k}\tilde{r}/2 \end{pmatrix}, \tag{1}$$

where $\underline{\tilde{v}}$ is the two-dimensional vector of velocity including one velocity component $\tilde{v}_z$ in $\tilde{z}$ direction and the other velocity component $\tilde{v}_r$ in $\tilde{r}$ direction. Furthermore, $\tilde{k}$ is the stretch rate imposed in the flame. For the considered flame configuration, where no curvature exists, flame stretch is a quantity that measures the amount of stretch of the flame surface due to the strain from the outer velocity field.

For the chemical reaction, a global one-step reaction $F \rightarrow P$ is considered, where F represents fuel and P product. In this chemical model, radicals are not included for simplicity, and the unburnt gas mixture is deficient in fuel so that only fuel concentration (fuel mass fraction $\tilde{Y}_F$) needs to be considered. Assuming a first-order chemical reaction, the corresponding reaction rate $\tilde{\omega}_F$ together with Arrhenius law [24, 25] reads $\tilde{\omega}_F = \tilde{\rho}\tilde{A}\tilde{Y}_F \exp\left(-\frac{\tilde{E}_a}{\tilde{R}\tilde{T}_g}\right)$, in which $\tilde{\rho}$ is the mixture density, $\tilde{A}$ the pre-exponent factor in Arrhenius law, $\tilde{E}_a$ the activation energy and $\tilde{R}$ the universal gas constant.

The diffusive mass flux for fuel is simply defined by Fick's laws of diffusion [24–26] as $\tilde{j}_F = -\tilde{\rho}\tilde{D}_F \frac{\mathrm{d}\tilde{Y}_F}{\mathrm{d}\tilde{z}}$, where $\tilde{D}_F$ denotes the molecular diffusion coefficient of fuel.

According to Han et al. [27], the diffusive-thermal model is employed to formulate the governing equations for temperature $\tilde{T}_g$ and fuel mass fraction $\tilde{Y}_F$. In this model, all thermodynamic and physical properties, including density $\tilde{\rho}$, isobaric specific heat capacity $\tilde{c}_p$, heat conductivity $\tilde{\lambda}_g$ of the mixture, and the molecular diffusion coefficient of fuel $\tilde{D}_F$, are assumed to be constant. Consequently, both governing equations can be expressed as

$$\tilde{\rho}\tilde{c}_p\tilde{v}_z\frac{\mathrm{d}\tilde{T}_g}{\mathrm{d}\tilde{z}} - \frac{\mathrm{d}}{\mathrm{d}\tilde{z}}\left(\tilde{\lambda}_g\frac{\mathrm{d}\tilde{T}_g}{\mathrm{d}\tilde{z}}\right) = \tilde{q}\tilde{\omega}_F, \tag{2}$$

$$\tilde{\rho}\tilde{v}_z\frac{\mathrm{d}\tilde{Y}_F}{\mathrm{d}\tilde{z}} - \frac{\mathrm{d}}{\mathrm{d}\tilde{z}}\left(\tilde{\rho}\tilde{D}_F\frac{\mathrm{d}\tilde{Y}_F}{\mathrm{d}\tilde{z}}\right) = -\tilde{\omega}_F, \tag{3}$$

where $\tilde{q}$ is the heat release per unit fuel mass due to chemical reaction.

The corresponding boundary conditions are formulated as:

1. at $\tilde{z} = 0$: this is the interface between the wall and flame. Since the one-step global reaction is assumed, the fuel is completely consumed to produce after the flame reaction sheet, and only the product exists in the burnt regime. Thus, the temperature and fuel mass fraction here are

$$\tilde{T}_g(\tilde{z} = 0) = \tilde{T}_c\,, \quad \tilde{Y}_F(\tilde{z} = 0) = 0. \tag{4}$$

Note that the contact temperature $\tilde{T}_c$ between plane wall and flame at this position needs to be determined later.

2. at $\tilde{z} \to +\infty$: this regime describes the thermo-kinetic state of the unburnt gas mixture, and thus

$$\tilde{T}_g(\tilde{z} \to +\infty) = \tilde{T}_0\,, \quad \tilde{Y}_F(\tilde{z} \to +\infty) = \tilde{Y}_{F,u}, \tag{5}$$

where $\tilde{T}_0$ is the temperature of fresh unburnt gas mixture, and $\tilde{Y}_{F,u}$ is the fuel mass fraction in the fresh mixture

To obtain the non-dimensional governing equations, the following non-dimensional variables are introduced:

$$z = \frac{\tilde{z}}{\tilde{\delta}_f^0}\,, \quad v_z = \frac{\tilde{v}_z}{\tilde{S}_L^0}\,, \quad T = \frac{\tilde{T}_g - \tilde{T}_0}{\tilde{T}_{ad} - \tilde{T}_0}\,, \quad Y_F = \frac{\tilde{Y}_F}{\tilde{Y}_{F,u}}\,, \quad \omega = \frac{\tilde{\omega}\tilde{\delta}_f^0}{\tilde{\rho}\tilde{S}_L^0\tilde{Y}_{F,u}}\,, \quad k = \tilde{k}\frac{\tilde{\delta}_f^0}{\tilde{S}_L^0}, \tag{6}$$

where the characteristic velocity $\tilde{S}_L^0$, characteristic length $\tilde{\delta}_f^0$ and characteristic temperature $\tilde{T}_{ad}$ reflect laminar burning velocity, flame thickness and adiabatic flame temperature of an unstretched planar flame with $\tilde{\delta}_f^0 = \tilde{\lambda}_g/(\tilde{\rho}\tilde{c}_p\tilde{S}_L^0)$ and $\tilde{T}_{ad} = \tilde{T}_0 + \tilde{Y}_{F,u}\tilde{q}/\tilde{c}_p$ respectively. Based on these non-dimensional variables, the corresponding non-dimensional governing equations [27] are

$$\frac{\mathrm{d}^2T}{\mathrm{d}z^2} + kz\frac{\mathrm{d}T}{\mathrm{d}z} + \omega = 0, \tag{7}$$

$$\frac{1}{Le}\frac{\mathrm{d}^2Y_F}{\mathrm{d}z^2} + kz\frac{\mathrm{d}Y_f}{\mathrm{d}z} - \omega = 0, \tag{8}$$

in which Le is the Lewis number: $Le = \tilde{\lambda}_g/(\tilde{\rho}\tilde{c}_p\tilde{D}_F)$ [28, 29]. And the corresponding non-dimensional boundary conditions are:

$$z{=}0: \quad T = T_c\,, \quad Y_F = 0, \tag{9}$$

$$z{=}{+}\infty: \quad T = 0 \quad , \quad Y_F = 1. \tag{10}$$

The analytical solution can be obtained in the large activation energy asymptotic limit. For this limit, the flame thickness tends to zero and the chemical reaction zone is infinitely narrow so that the reaction rate can be replaced by the Delta function [30–33]:

$$\omega = \left[\alpha_f + (1-\alpha_f)T_f\right]^2 \exp\left[\frac{Ze}{2}\,\frac{T_f - 1}{\alpha_f + (1-\alpha_f)T_f}\right]\delta(z - z_f), \tag{11}$$

where $\alpha_f = \tilde{T}_0/\tilde{T}_{ad}$ is the thermal expansion ratio for flame and $Ze = \tilde{E}_a(1-\alpha_f)/(\tilde{R}\tilde{T}_{ad})$ the Zel'dovich number [28–30]. Typically, $Ze \sim \mathcal{O}(10)$ is reasonable for the combustion chemical reaction in the large activation energy asymptotic limit [28, 30].

Integrating the governing equations in the unburnt zone ($z \geq z_f$) and burnt zone ($0 \leq z \leq z_f$), and neglecting the nonlinear reaction term in ω due to the limit of large activation energy, the analytical asymptotic solution for the non-dimensional temperature distribution is

$$T(z) = \begin{cases} T_c + (T_f - T_c)\dfrac{\int_0^z e^{-k\xi^2/2}\mathrm{d}\xi}{\int_0^{z_f} e^{-k\xi^2/2}\mathrm{d}\xi} & \left(0 \leq z \leq z_f\right) \\ T_f\dfrac{\int_{z_f}^{+\infty} e^{-k\xi^2/2}\mathrm{d}\xi}{\int_z^{+\infty} e^{-k\xi^2/2}\mathrm{d}\xi} & \left(z \geq z_f\right) \end{cases}. \tag{12}$$

TABLE 1 General 3D equations of motion and for heat conduction (left column) and corresponding simplified 1D equations under steady state with constant material properties and without body force.

General 3D equations	Simplified stationary 1D equations
$\left(\tilde{K}_0+\frac{1}{3}\tilde{G}_0\right)\frac{\mathrm{d}^2\tilde{u}_j}{\mathrm{d}\tilde{x}_j\mathrm{d}\tilde{x}_i}+\tilde{G}_0\frac{\mathrm{d}^2\tilde{u}_i}{\mathrm{d}\tilde{x}_j\mathrm{d}\tilde{x}_i}-\tilde{\beta}_0\frac{\mathrm{d}\tilde{T}_s}{\mathrm{d}\tilde{x}_i}=\tilde{\rho}_0\frac{\partial^2\tilde{u}_i}{\partial\tilde{t}^2}$	$\left(\tilde{K}_0+\frac{4}{3}\tilde{G}_0\right)\frac{\mathrm{d}^2\tilde{u}_1}{\mathrm{d}\tilde{x}_1^2}-\tilde{\beta}_0\frac{\mathrm{d}\tilde{T}_s}{\mathrm{d}\tilde{x}_1}=0$
$\tilde{\lambda}_s\frac{\mathrm{d}^2\tilde{T}_s}{\mathrm{d}\tilde{x}_i\mathrm{d}\tilde{x}_i}-\tilde{T}_0\tilde{\beta}_0\frac{\partial}{\partial\tilde{x}_i}\left(\frac{\partial\tilde{u}_i}{\partial\tilde{t}}\right)=\tilde{\rho}_0\tilde{c}_0\frac{\partial\tilde{T}_s}{\partial\tilde{t}}$	$\tilde{\lambda}_s\frac{\mathrm{d}^2\tilde{T}_s}{\mathrm{d}\tilde{x}_1^2}=0$

In these equations, z_f is the flame position and T_f the maximum flame temperature. Taking into account the jump relation at the flame front z_f [27], the following algebraic system of equations is obtained for z_f and T_f:

$$(T_f-T_c)\frac{e^{-kz_f^2/2}}{\int_0^{z_f}e^{-k\xi^2/2}\mathrm{d}\xi}+T_f\frac{e^{-kz_f^2/2}}{\int_{z_f}^{+\infty}e^{-k\xi^2/2}\mathrm{d}\xi}=\frac{1}{Le}\frac{e^{-kLez_f^2/2}}{\int_{z_f}^{+\infty}e^{-kLe\xi^2/2}\mathrm{d}\xi}=\left[\alpha_f+(1-\alpha_f)T_f\right]^2\exp\left[\frac{Ze}{2}\frac{T_f-1}{\alpha_f+(1-\alpha_f)T_f}\right]. \tag{13}$$

In these algebraic equations, the stretch rate k is an *a-priori* given quantity, and z_f and T_f are funtion of k: $z_f=z_f(k)$ and $T_f=T_f(k)$. With the information of z_f, the flame speed can be easily determined as $S_L=k\,z_f$.

2.2 | Model for thermo-elasticity in the plane wall

In our analysis, the plane wall is modeled as an isotropic thermo-elastic solid with isotropic heat conduction. The combustion-induced strain inside the wall is assumed to be small, allowing the application of a geometrically linear thermo-elasticity theory. The wall is assumed to be infinite in the $\tilde{x}_2$ and $\tilde{x}_3$ directions, with displacement occurring only in the $\tilde{x}_1$ direction. Additionally, the temperature and displacement fields in the plane wall are assumed to be dependent solely on the $\tilde{x}_1$-coordinate $(\tilde{T}_s(\tilde{x}_1),\tilde{u}_1(\tilde{x}_1))$. No body force and external energy source are applied in the plane wall, and for simplicity, all material properties are assumed to be constant, including the bulk modulus $\tilde{K}_0$, shear modulus $\tilde{G}_0$, the heat conductivity $\tilde{\lambda}_s$, and $\tilde{\beta}_0=3\tilde{K}_0\tilde{\alpha}_s$ representing the thermal stress induced by the temperature change with $\tilde{\alpha}_s$ the coefficient of thermal expansion.

In Table 1(left column), the general 3D equations for heat conduction without external energy source and the equation of motion without body force are listed. In these equations, all material properties are considered constant. In both equations, $\frac{\partial\tilde{u}_i}{\partial\tilde{t}}$ and $\frac{\partial\tilde{T}_s}{\partial\tilde{t}}$ represent the first time derivative of displacement and temperature, respectively, and $\frac{\partial^2\tilde{u}_i}{\partial\tilde{t}^2}$ represents the second time derivative of displacement. Based on the aforementioned assumptions and simplifications, and considering the entire process under equilibrium (steady state), the 3D equations can be simplified, as listed in Table 1 (right column).

Note that although the displacement in our study is simplified to 1D situation, the corresponding stress is 3D. If the temperature difference and displacement are known, the stress tensor is given by

$$\underline{\tilde{\sigma}}=-\tilde{\beta}_0(\tilde{T}_s-\tilde{T}_0)\begin{pmatrix}1&0&0\\0&1&0\\0&0&1\end{pmatrix}+\frac{\mathrm{d}\tilde{u}_1}{\mathrm{d}\tilde{x}_1}\begin{pmatrix}\tilde{K}_0+\frac{4}{3}\tilde{G}_0&0&0\\0&\tilde{K}_0-\frac{2}{3}\tilde{G}_0&0\\0&0&\tilde{K}_0-\frac{2}{3}\tilde{G}_0\end{pmatrix}. \tag{14}$$

For the considered model for the plane wall, the following boundary conditions are applied:

1. At $\tilde{x}_1=0$: At the contact surface, the contact temperature $\tilde{T}_c$ will be determined together with the flame temperature (see below). The traction at the surface is equal to the negative pressure induced by the flame:

$$\tilde{T}_s(\tilde{x}_1=0)=\tilde{T}_c,\quad \tilde{\sigma}_{11}(\tilde{x}_1=0)=-\tilde{p}_g. \tag{15}$$

2. At $\tilde{x}_1 = \tilde{H}$: a fixed temperature $\tilde{T}_0$ is assumed and the displacement is set equal to zero:

$$\tilde{T}_s(\tilde{x}_1 = \tilde{H}) = \tilde{T}_0, \quad \tilde{u}_1(\tilde{x}_1 = \tilde{H}) = 0. \tag{16}$$

In the following, non-dimensional variables are introduced:

$$u_1 = \frac{\tilde{u}_1}{\tilde{u}_c}, \quad x_1 = \frac{\tilde{x}_1}{\tilde{H}}, \quad \theta = \frac{\tilde{T}_s - \tilde{T}_0}{\tilde{T}_{ad} - \tilde{T}_0}, \quad \tilde{u}_c = \frac{\tilde{\beta}_0(\tilde{T}_{ad} - \tilde{T}_0)\tilde{H}}{\tilde{G}_0}. \tag{17}$$

Then the non-dimensional governing equations for the temperature and the displacement in the solid read

$$\frac{2(1-\nu)}{1-2\nu}\frac{\mathrm{d}^2 u_1}{\mathrm{d}x_1^2} - \frac{\mathrm{d}\theta}{\mathrm{d}x_1} = 0, \tag{18}$$

$$\frac{\mathrm{d}^2\theta}{\mathrm{d}x_1^2} = 0, \tag{19}$$

in which ν refers to Poisson's ratio describing the ratio of lateral contraction to longitudinal extension of the material under longitudinal tensile stress [34]. Note that here the Poisson's ratio can be used to describe the ratio between $\tilde{K}_0$ and $\tilde{G}_0$, namely $\tilde{K}_0/\tilde{G}_0 = \frac{2}{3}(1+\nu)/(1-2\nu)$, due to the assumption of linear elastic behavior and isotropic solid [34, 35]. And the corresponding non-dimensional boundary conditions are:

$$x_1{=}0: \quad \theta = T_c, \quad \sigma_{11} = -p_g, \tag{20}$$

$$x_1{=}1: \quad \theta = 0, \quad u_1 = 0. \tag{21}$$

By further introducing the characteristic stress $\tilde{\sigma}_c = \tilde{\beta}_0(\tilde{T}_{ad} - \tilde{T}_0)$, the non-dimensional stress tensor $\sigma_{ij} = \tilde{\sigma}_{ij}/\tilde{\sigma}_c$ reads

$$\underline{\underline{\sigma}} = -\theta\begin{pmatrix}1&0&0\\0&1&0\\0&0&1\end{pmatrix} + \frac{\mathrm{d}u_1}{\mathrm{d}x_1}\begin{pmatrix}\frac{2(1-\nu)}{1-2\nu}&0&0\\0&\frac{2\nu}{1-2\nu}&0\\0&0&\frac{2\nu}{1-2\nu}\end{pmatrix}. \tag{22}$$

Considering the boundary conditions for the solid, one obtains the analytical solution for temperature field and the non-dimensional stress tensor as

$$\theta = T_c(1-x_1), \qquad \underline{\underline{\sigma}} = -T_c(1-x_1)\begin{pmatrix}0&0&0\\0&\frac{1-2\nu}{1-\nu}&0\\0&0&\frac{1-2\nu}{1-\nu}\end{pmatrix} - p_g\begin{pmatrix}1&0&0\\0&\frac{\nu}{1-\nu}&0\\0&0&\frac{\nu}{1-\nu}\end{pmatrix}. \tag{23}$$

After the stress tensor is obtained, the von Mises equivalent stress σ_{vM} is determined by the Frobenius norm of the traceless part of the stress tensor as [36]:

$$\sigma_{\mathrm{vM}}^2 = \frac{3}{2}\sigma_{ij}^{\mathrm{dev}}\sigma_{ij}^{\mathrm{dev}}, \qquad \text{with } \sigma_{ij}^{\mathrm{dev}} = \sigma_{ij} - \frac{1}{3}\sigma_{kk}\delta_{ij}, \tag{24}$$

where $\sigma_{ij}^{\mathrm{dev}}$ is the stress deviator.

2.3 | Coupling at contact surface

Both models are coupled through the contact temperature between the flame and the plane wall. At the contact surface, the contact temperature must be equal from both sides: $T_c(z=0) = T_c(x_1 = 0)$. Furthermore, the heat flux from both

TABLE 2 Non-dimensional parameters and variables.

Gas phase: Flame		
T_f	Flame temperature	(to be determined)
z_f	Flame position	(to be determined)
Ze	Zel'dovich number	$Ze = 10$
α_f	Thermal expansion ratio	$\alpha_f = 0.22$
Le	Lewis number	$0.4 \leq Le \leq 3.0$
k	Stretch rate	$k \leq k_{\text{ext}}$
Solid phase: Plane wall		
$\sigma_{\text{vM}}^{\max}$	Max. von Mises equivalent stress	(to be determined)
ν	Poisson's ratio	$\nu = 0.3$
Contact surface		
T_c	Contact temperature	(to be determined)
R_{sg}	ratio of thermal resistance	$\mathcal{O}(0)$ - $\mathcal{O}(10^0)$

sides must also be identical, which can be written in form with dimension:

$$-\tilde{\lambda}_g \left.\frac{\mathrm{d}\tilde{T}_g}{\mathrm{d}\tilde{z}}\right|_{\tilde{z}=0} = +\tilde{\lambda}_s \left.\frac{\mathrm{d}\tilde{T}_s}{\mathrm{d}\tilde{x}_1}\right|_{\tilde{x}_1=0}. \tag{25}$$

Note that different signs have been used from both sides, because $z-$ and x_1-coordinate point in opposite directions (cf. Figure 1). Together with the introduced non-dimensional variables mentioned above, the non-dimensional form for the boundary condition in terms of equal heat flux is

$$-R_{sg} \left.\frac{\mathrm{d}T}{\mathrm{d}z}\right|_{z=0} = \left.\frac{\mathrm{d}T}{\mathrm{d}x_1}\right|_{x_1=0}, \tag{26}$$

in which $R_{sg} = \tilde{R}_s/\tilde{R}_g$ compares the ratio of thermal resistance of solid ($\tilde{R}_s = \tilde{H}/\tilde{\lambda}_s$) and of flame ($\tilde{R}_g = \tilde{\delta}_f^0/\tilde{\lambda}_g$).

Combining the analytical solution of temperature for both flame (Equation 12) and solid (Equation 23), the non-dimensional contact temperature can be determined by an algebraic equation

$$T_c = \frac{R_{sg}\, T_f}{R_{sg} + \int_0^{z_f} e^{-k\xi^2/2}\mathrm{d}\xi}. \tag{27}$$

3 | RESULTS AND DISCUSSION

In this study, our emphasis is on exploring how the gas mixture (expressed in terms of Lewis number) and flow conditions (indicated by stretch rate) influence the induced thermo-mechanical stress. Table 2 provides a comprehensive list of non-dimensional parameters and variables, along with their corresponding selected values or ranges, or they are to be determined as output values. Before delving into the results, it is pertinent to note a few considerations regarding the varied parameters and variables:

1. The Zeldovich number $Ze = 10$ and thermal expansion ratio for the flame $\alpha_f = 0.22$ are maintained as constant values. These are reference values, and the composition of the gas mixture (such as varying hydrogen content) has a negligible impact on these two parameters, as indicated in other literature [37, 38]. The chosen values are consistent with those applied in other analyses [27, 28, 30].
2. We are considering a range of Le numbers that cover a wide spectrum of possible combustible mixtures applicable in real combustion scenarios:
   A. Pure hydrogen/air mixture typically has a Lewis number around $Le \approx 0.4$ [39]. For pure CH_4/air or NH_3/air mixtures, the corresponding $Le \approx 1$ [40, 41]. The regime $Le \leq 1$ is consistent with gas mixtures containing methane,

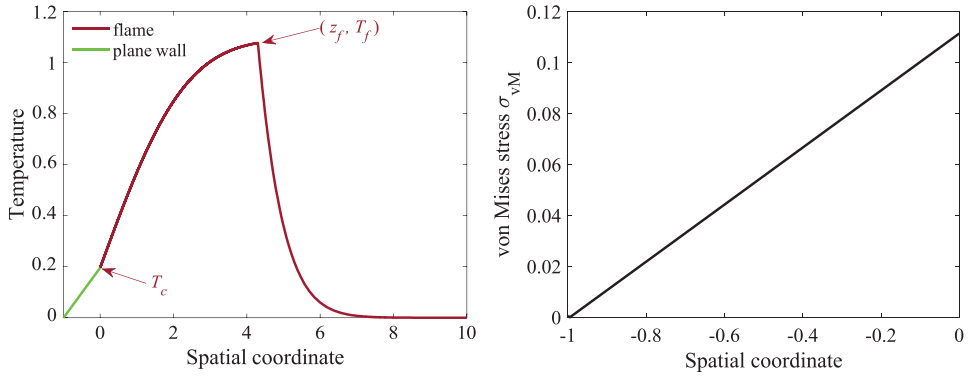

FIGURE 2 Typical spatial profiles for temperature (left) and von Mises stress (right) with parameter values $Le = 0.5$ and $R_{sg} = 0.5$.

syngas, or ammonia enriched with hydrogen [42–44]. As more hydrogen is added to the gas mixture, the Lewis number decreases.

B. Most HC fuels have a Lewis number greater than 1 ($Le > 1$) [45–47]. In the case of a lean mixture containing the primary reference automobile fuel (PRF), which is a blend of iso-octane and n-heptane with air, the corresponding Lewis number tends to be around 3 ($Le \approx 3.0$) [46].

3. The stretch rate is bounded by the extinction stretch rate k_{ext}, beyond which no stable burning flame can be sustained.
4. A typical range for Poisson's ratio ν in engineering alloys is around 0.2–0.35 [35, 48]. Since this parameter is only important for determining thermo-mechanical stress inside the plane wall and has no influence on the flame behavior, we set it as $\nu = 0.3$ throughout the entire study. This value is also reasonable for alloys such as Inconel 718 [49] and Ti-6Al-4V [50].
5. The ratio of thermal resistance R_{sg} is in order of magnitude $\mathcal{O}(0) - \mathcal{O}(10^0)$. This is based on the estimation that typical flame thickness for various hydrogen or HC flames is in order of magnitude $\mathcal{O}(10^{-1})$mm [51, 52] and a typical thickness of a rotor blade in the gas turbine combustor is in order of magnitude $\mathcal{O}(10^1) - \mathcal{O}(10^2)$mm [53, 54].

Typical spatial profiles for temperature over the entire domain (left) and von Mises stress inside the plane wall (right) are presented in Figure 2. The contact temperature T_c corresponds to the temperature at $x_1 = z = 0$. Since the heat conductivity of the wall is assumed to be a constant value, the temperature distribution inside the plane wall is a linear function over the spatial coordinate, increasing from 0 to T_c. The flame has the maximum temperature T_f (flame temperature) at the flame position z_f. Consistent with the temperature profile, the von Mises equivalent stress σ_{vM} reaches its maximum at the contact surface.

3.1 | Variation of Lewis number *Le*

In this section, we will discuss the effect of the Lewis number (Le) on the flame and thermo-mechanical stress in the plane wall. It should be reiterated that a smaller Le number corresponds to a higher hydrogen content in the combustible gas mixture.

Figure 3 illustrates the flame position z_f, flame temperature T_f, and flame speed S_L in relation to the stretch rate k under different Lewis numbers (Le). All curves terminate at the extinction stretch rate, beyond which no stable burning flame can be sustained. It is worth noting that the impact of the stretch rate on these flame parameters has been extensively studied in ref. [9]. The primary difference lies in the fixed temperature condition at the wall in their work, specified as $T(z = 0) = \theta(x_1 = 0) = 0$. Nevertheless, our observations indicate that the general trends persist even when considering the contact temperature. Therefore, we will briefly summarize the effect of the stretch rate on the flame parameters, with more detailed discussions available in ref. [9].

In general, irrespective of the Lewis number, an increase in the stretch rate causes the flame to move closer to the plane wall, resulting in a decrease in the flame position. Flame extinction happens when the flame approaches the wall, leading to increased heat loss to the wall. If the flame loses enough heat such that the heat release from the chemical reaction can no longer sustain the reaction, the reaction rate decreases, ultimately resulting in flame extinction.

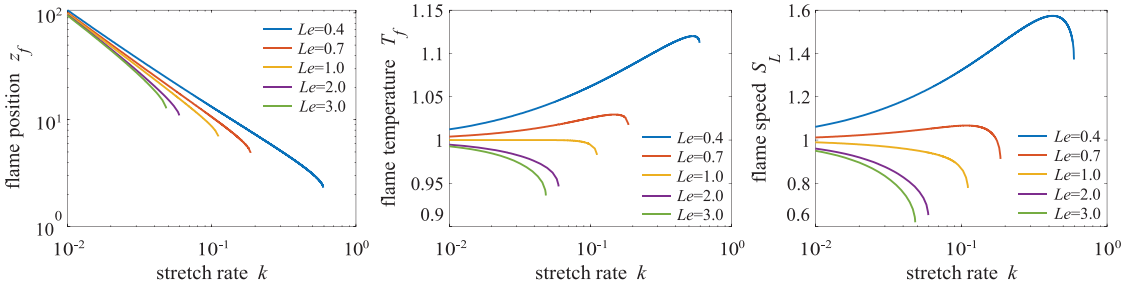

FIGURE 3 Dependence of flame position z_f, flame temperature T_f and flame speed S_L on stretch rate k with $R_{sg} = 0.5$.

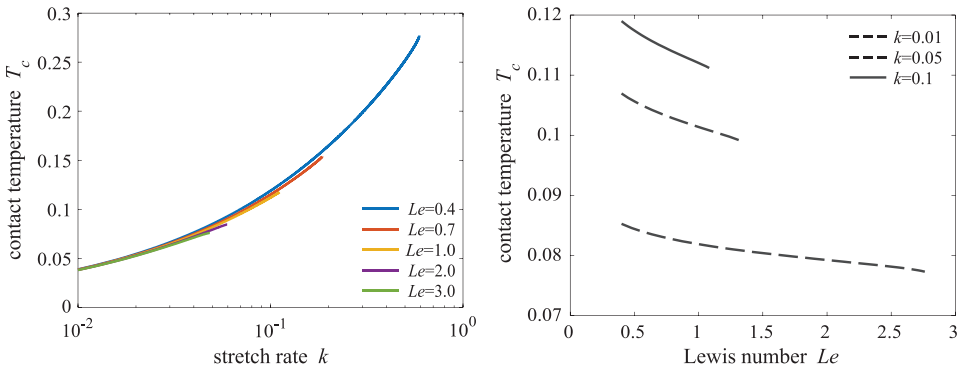

FIGURE 4 Dependence of contact temperature T_c on stretch rate k (left) and on the Lewis number Le. Conditions are same as in Figure 3.

The behavior of flame temperature T_f with varying Lewis number from Figure 3(middle) is more complicated:

1. for $Le < 1$: the chemical reaction rate ω increases with an increasing stretch rate k [9, 55], causing an increase in flame temperature. As the flame approaches the plane wall, the heat loss from the flame to the wall intensifies, resulting in a decrease in flame temperature until extinction. Furthermore, for the positively stretched premixed flames, $Le \leq 1$, flame temperature is higher than the adiabatic flame temperature, which is also reported in refs. [29, 56].
2. For $Le > 1$: the chemical reaction rate decreases with an increasing stretch rate [9, 55]. Even when the flame front is still far from the plane wall, where heat loss still has little effect on the flame, the chemical reaction rate decreases to a certain value below which no further chemical reaction can be sustained. This also explains why mixtures with $Le > 1$ exhibit a smaller extinction limit than mixtures with $Le < 1$. Moreover, for the negatively stretched premixed flames, $Le > 1$, flame temperature is lower than the adiabatic flame temperature, consistent with the analysis in ref. [29].

The influence of the Lewis number on flame properties, such as flame temperature and extinction limit, suggests that incorporating lighter molecules (e.g., hydrogen) in the gas mixture enhances combustion efficiency by increasing the flame temperature and improving the extinction limit. This aligns with nowadays approaches to the application of hydrogen-enriched combustion systems [57–59].

Focusing on the solid plane wall, Figure 4 illustrates the dependence of the contact temperature T_c on the stretch rate k (left subfigure) and on the Lewis number Le for specific stretch rates (right subfigure), under the same conditions as in Figure 3. As the flame approaches closer to the plane wall with an increasing stretch rate, the contact temperature shows a significant rise due to the higher impact of the flame temperature. While the stretch rate shows a noticeable influence on the contact temperature, the role of the Lewis number is comparatively minor. To be more precise, the contact temperature exhibits a slight decrease with increasing Lewis number (in the present work, only around 10% decrease). This occurs because for flames with a larger Le number, on one side, the flame moves closer to the wall (resulting in a smaller flame position, cf. Figure 3), while on the other side, the flame has a lower flame temperature (cf. Figure 3). These two phenomena compensate for each other, resulting in the effect of the Le number on the contact temperature becoming smaller.

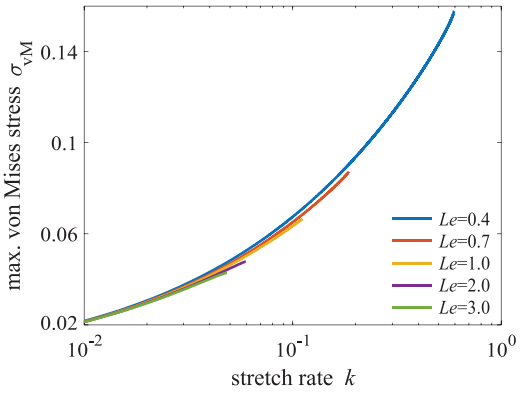

FIGURE 5 Dependence of maximum von Misess stress σ_{wM}^{max} on stretch rate k with $R_{sg} = 0.5$.

Figure 5 compares the maximum von Mises stress σ_{wM}^{max} against stretch rate k for various Lewis numbers. The trend agrees with the observation from the contact temperature, indicating that σ_{wM}^{max} is significantly impacted by the stretch rate and minimally influenced by the Lewis number of the fuel mixture. This provides us with several practical insights for the construction of combustion applications:

1. For most HC fuels involving heavy molecules ($Le > 1.0$), an increase in flow velocity (indicated by the stretch rate) leads to elevated thermo-mechanical stress and reduced flame temperature.
2. For fuels involving small or light molecules ($Le < 1.0$), even though an increase in flow velocity (indicated by the stretch rate) leads to elevated thermo-mechanical stress, the flame temperature can become higher, thus improving combustion efficiency simultaneously.
3. More interestingly, if the flow velocity remains unchanged, the thermo-mechanical stress inside the solid will not be affected by the fuel type. However, using a fuel with a smaller Lewis number would achieve a higher flame temperature and enhanced combustion efficiency. In practical applications, conventional fuels under hydrogen enrichment conditions are widely recognized for their improved combustion efficiency and, based on the results here, would only slightly increase thermo-mechanical stress as well.

3.2 | Variation of ratio of thermal resistance R_{sg}

In this section, we will discuss the effect of the thermal resistance ratio (R_{sg}) on the flame properties and thermo-mechanical stress in the plane wall. It should be mentioned here at first that, according to Equation (27), the contact temperature T_c tends to zero ($T_c = 0$) if $R_{sg} \to 0$, corresponding to a small thermal resistance of the solid. On the other hand, the contact temperature tends to the flame temperature ($T_c = T_f$) if $R_{sg} \to +\infty$, corresponding to a high thermal resistance of the solid. Note that, in general, the higher the thermal resistance, the lower the heat loss.

Figures 6 and 7 illustrate the flame position z_f, flame temperature T_f, and flame speed S_L in relation to the stretch rate k under different R_{sg} numbers for fuels with small Le number and large Le number. In general, it is observed that the extinction stretch rate increases with increasing R_{sg}. In other words, with the increase of R_{sg}, the flame becomes more stable against extinction. This is straightforward, as the increase of R_{sg} corresponds to a higher thermal resistance of the solid. A higher thermal resistance means a greater resistance to heat transfer, leading to lower heat loss of flame through the plane wall. Therefore, the flame loses less heat and becomes more stable.

However, it is observed that the influence of R_{sg} on flame properties is larger for fuels with small Le numbers, while it is relatively small for fuels with large Le numbers. This can be explained as follows: if the rate of thermal diffusion is larger than the rate of mass diffusion ($Le > 1$), heat is transferred faster outwards to heat up the unburnt gas, and the consumption of fuel is mainly controlled by the convection process ($\frac{1}{Le}\frac{d^2Y_F}{dz^2} \to 0$ in Equation (8)). Since the heat transport through the plane wall is not affected by the convective process, most flame properties at larger Le numbers are not significantly dependent on R_{sg}.

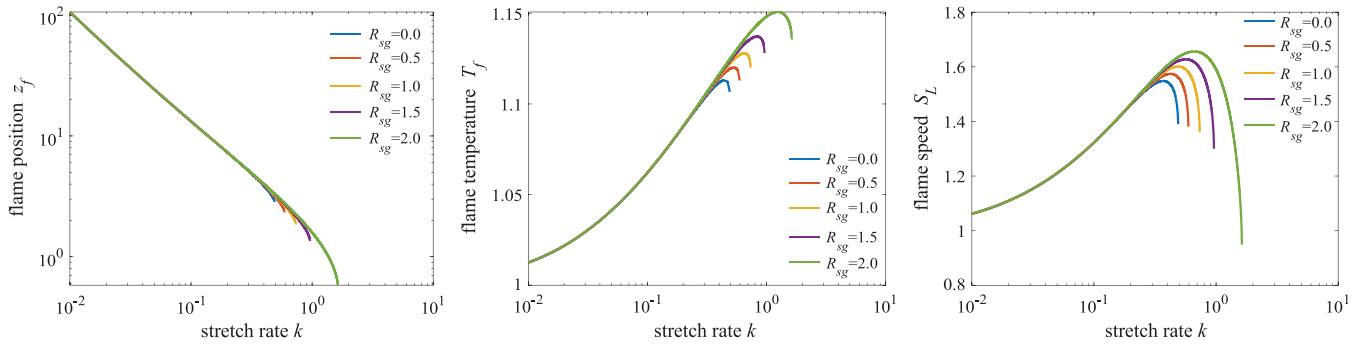

FIGURE 6 Dependence of flame position z_f, flame temperature T_f and flame speed S_L on stretch rate k with $Le = 0.4$.

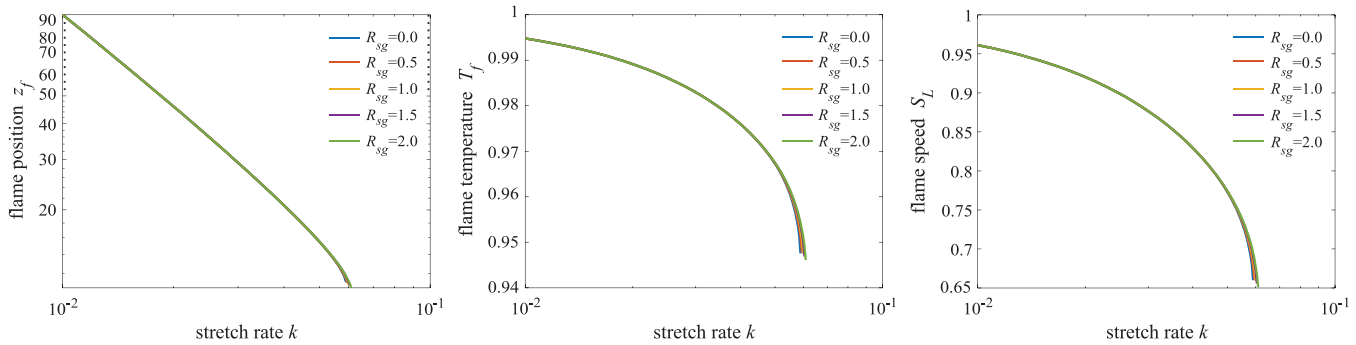

FIGURE 7 Dependence of flame position z_f, flame temperature T_f and flame speed S_L on stretch rate k with $Le = 2.0$.

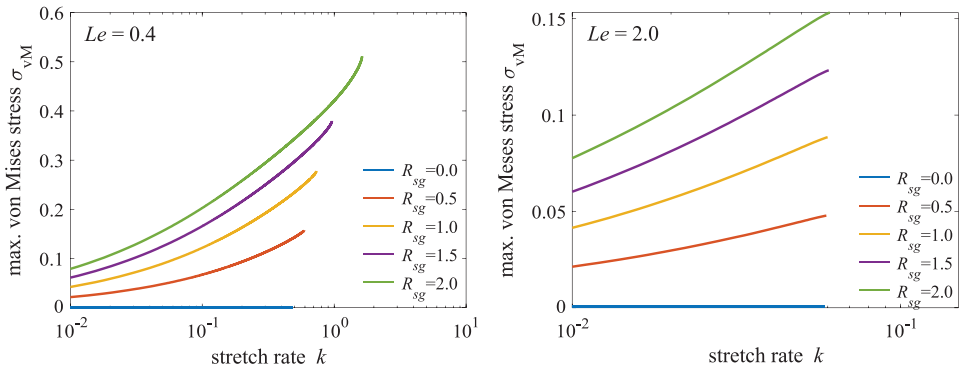

FIGURE 8 Dependence of maximum of von Misess stress σ_{vM}^{max} on stretch rate k with different R_{sg} for $Le = 0.4$ (left) and $Le = 2.0$ (right).

Moreover, we observe that at low stretch rates, which are far away from the extinction limit, the flame properties are not affected by R_{sg}. Only when the stretch rate approaches the extinction limit does the influence of R_{sg} become noticeable. This is because if the stretch rate is small, the flame is located far from the plane wall, so the plane wall has a minor effect on the flame. The effect of heat loss through the plane wall on the flame becomes more important as the flame approaches the plane wall with increasing stretch rate.

Although thermal resistance is only significant for flame under certain conditions, the results presented in Figure 8 demonstrate that variations in R_{sg} play a significant role in the maximum von Misess stress. According to Equation (27), $T_c \to 0$ as $R_{sg} \to 0$, indicating a zero temperature gradient inside the wall. Consequently, there is no thermal expansion, and the corresponding thermo-mechanical stress vanishes (blue lines in Figure 8). Conversely, in the limit as $R_{sg} \to \infty$, $T_c \to T_f$ according to Equation (27), resulting in a noticeable temperature gradient inside the plane wall (increase from ambient temperature to flame temperature). Thus, as R_{sg} increases, the thermo-mechanical stress inside the wall becomes larger.

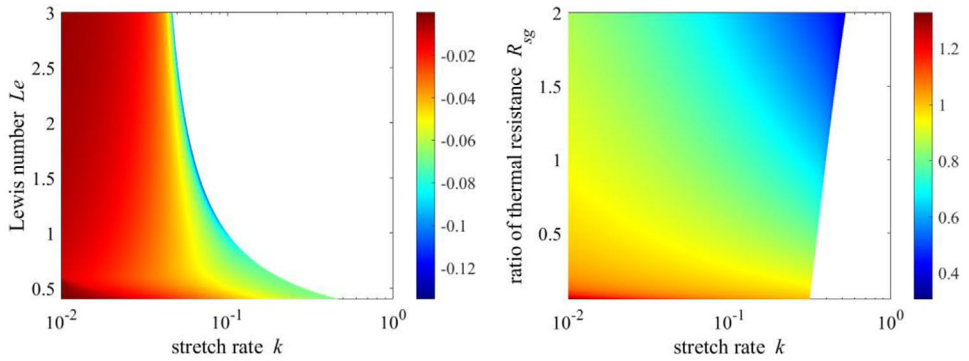

FIGURE 9 Contour plot of the sensitivity of maximum of von Misess stress $\sigma_{\mathrm{vM}}^{\max}$ with respect to the Lewis number Le (left) and to ratio of thermal resistance R_{sg} (right).

3.3 | Sensitivity analysis of max. von Mises stress

Previous two sections discussed the effect of Lewis number Le and ratio of thermal resistance R_{sg} on the maximum of von Misess stress $\sigma_{\mathrm{vM}}^{\max}$. In this part, we briefly summarize it by further performing the sensitivity analysis. Contour plots of the sensitivity of maximum of von Misess stress $\sigma_{\mathrm{vM}}^{\max}$ with respect to Lewis number Le (left) and to ratio of thermal resistance R_{sg} (right) are illustrated in Figure 9. The sensitivity value is determined by using the bruto force method. For example, the sensitivity of $\sigma_{\mathrm{vM}}^{\max}$ with respect to Le number is calculated as

$$
\begin{aligned}
S_{Le}^{\mathrm{rel}} &= \frac{Le}{\sigma_{\mathrm{vM}}^{\max}} \cdot \frac{\partial \sigma_{\mathrm{vM}}^{\max}}{\partial Le} \quad \text{(evaluated by finite difference)} \\
&\approx \frac{Le}{\sigma_{\mathrm{vM}}^{\max}} \cdot \frac{\Delta \sigma_{\mathrm{vM}}^{\max}}{\Delta Le} = \frac{Le}{\sigma_{\mathrm{vM}}^{\max}} \cdot \frac{\sigma_{\mathrm{vM}}^{\max}(1.1k_r) - \sigma_{\mathrm{vM}}^{\max}(Le)}{1.1Le - Le} = 10 \times \frac{\sigma_{\mathrm{vM}}^{\max}(1.1Le) - \sigma_{\mathrm{vM}}^{\max}(Le)}{\sigma_{\mathrm{vM}}^{\max}(Le)}.
\end{aligned} \tag{28}
$$

Consistent with the results in Figure 5, the negative sensitivity of $\sigma_{\mathrm{vM}}^{\max}$ with respect to the Lewis number Le shows that an increase in Le number decreases the thermo-mechanical stress. However, such sensitivity is relatively low, and the maximum sensitivity value is only around -0.14%, indicating that under the same flow condition (here represented by stretch rate), using fuels with lighter molecules results in a minor increase in the thermo-mechanical stress. However, $\sigma_{\mathrm{vM}}^{\max}$ is more sensitive to R_{sg}, as the thermal resistance has a significant influence on the temperature distribution inside the plane wall. Therefore, it is concluded from this simple sensitivity analysis that for the construction and design of combustor components, the variation of fuels may not require reconsideration of the thermo-mechanical stress issue.

4 | CONCLUSIONS

The flame-solid interaction is theoretically modeled and analyzed based on a steady laminar stagnation flow flame stabilized at a plane wall. The heat conduction through the plane wall is considered, and a thermo-elasticity model is used to investigate the thermo-mechanical stress inside the wall. Analytical solutions for the flame and plane wall are proposed in the present work by considering the dimensionless forms of the corresponding simplified governing equations. The results show that the Lewis number has a minor effect on the thermo-mechanical stress, while the thermal resistance has a significant effect. As ongoing research, the theoretical analysis will be extended to consider the elasto-plastic strain of the material.

ACKNOWLEDGMENTS

Chunkan Yu acknowledges financial support by the DFG (project H2MAT3D, project no. 523879740 within the DFG-SPP 2419 HyCAM). Zheng Chen acknowledges financial support by National Natural Science Foundation of China (No. 52176096).

Open access funding enabled and organized by Projekt DEAL.

ORCID

Chunkan Yu https://orcid.org/0000-0002-0550-5003

REFERENCES

[1] Alkidas, A.: Combustion-chamber crevices: the major source of engine-out hydrocarbon emissions under fully warmed conditions. Prog. Energy Combust. Sci. 25(3), 253–273 (1999)
[2] Mukai, K., Miyazaki, H.: The influence of the combustion chamber head material of a gasoline engine on exhaust HC. SAE Trans. 2119–2126 (2000)
[3] Zhu, Y.M., Gong, Y., Yang, Z.G.: Failure analysis on over-temperature combustion of transformers in 4 MW offshore wind turbines. Eng. Fail. Anal. 96, 211–222 (2019)
[4] González, M.S., Rojas-Hernández, I.: Hydrogen embrittlement of metals and alloys in combustion engines. Tecnol. Marcha 31(2), 3–13 (2018)
[5] Nazari, M.A., Alavi, M.F., Salem, M., Assad, M.E.H.: Utilization of hydrogen in gas turbines: A comprehensive review. Int. J. Low Carbon Technol. 17, 513–519 (2022)
[6] Sharma, K., Aditya, A., Srinivas, G.: Material failure analysis and engine combustion instabilities of both air and non-air breathing engines. Mater. Today: Proc. 27, 231–237 (2020)
[7] Mark, C.P., Selwyn, A.: Design and analysis of annular combustion chamber of a low bypass turbofan engine in a jet trainer aircraft. Propuls. Power Res. 5(2), 97–107 (2016)
[8] Sohn, C.H., Park, I.S., Kim, S.K., Kim, H.J.: Acoustic tuning of gas–liquid scheme injectors for acoustic damping in a combustion chamber of a liquid rocket engine. J. Sound Vib. 304(3-5), 793–810 (2007)
[9] Law, C.: Dynamics of stretched flames. Symp. (Int.) Combust. 22(1), 1381–1402 (1989)
[10] Tsuji, H., Yamaoka, I.: Structure and extinction of near-limit flames in a stagnation flow. Symp. (Int.) Combust. 19(1), 1533–1540 (1982)
[11] Popp, P., Baum, M.: Analysis of wall heat fluxes, reaction mechanisms, and unburnt hydrocarbons during the head-on quenching of a laminar methane flame. Combust. Flame 108(3), 327–348 (1997)
[12] Boust, B., Sotton, J., Labuda, S., Bellenoue, M.: A thermal formulation for single-wall quenching of transient laminar flames. Combust. Flame 149(3), 286–294 (2007)
[13] Dabireau, F., Cuenot, B., Vermorel, O., Poinsot, T.: Interaction of flames of H2+ O2 with inert walls. Combust. Flame 135(1-2), 123–133 (2003)
[14] Zirwes, T., Häber, T., Zhang, F., et al.: Numerical study of quenching distances for side-wall quenching using detailed diffusion and chemistry. Flow Turbul. Combust. 106, 649–679 (2021)
[15] Xia, Y., Sharkey, P., Verma, I., Khaware, A., Cokljat, D.: Prediction of Thermoacoustic Instability and Fluid–Structure Interactions for Gas Turbine Combustor. J. Eng. Gas Turbines Power 144(9), 091005 (2022)
[16] Yu, C., Böhlke, T., Medina, A.V., Yang, B., Maas, U.: Flame–Solid interaction: Thermomechanical analysis for a steady laminar stagnation flow stoichiometric nh3–h2 flame at a plane wall. Energy Fuels 37(4), 3294–3306 (2023)
[17] Yu, C., Srikanth, S., Böhlke, T., Gorr, B., Maas, U.: Steady laminar stagnation flow NH3-H2-air flame at a plane wall: Flame extinction limit and its influence on the thermo-mechanical stress and corrosive behavior of wall materials. Appl. Energy Combust. Sci. 18, 100261 (2024)
[18] Nabi, M.N.: Theoretical investigation of engine thermal efficiency, adiabatic flame temperature, NOx emission and combustion-related parameters for different oxygenated fuels. Appl. Therm. Eng. 30(8-9), 839–844 (2010)
[19] Aliyu, M., Abdelhafez, A., Nemitallah, M.A., Said, S.A., Habib, M.A.: Effects of adiabatic flame temperature on flames' characteristics in a gas-turbine combustor. Energy 243, 123077 (2022)
[20] Mishra, S., Dahiya, R.: Adiabatic flame temperature of hydrogen in combination with gaseous fuels. Int. J. Hydrogen Energy 14(11), 839–844 (1989)
[21] Chao, B., Law, C.: Asymptotic theory of flame extinction with surface radiation. Combust. Flame 92(1-2), 1–24 (1993)
[22] Davis, S., Quinard, J., Searby, G.: Determination of Markstein numbers in counterflow premixed flames. Combust. Flame 130(1-2), 112–122 (2002)
[23] Ju, Y., Masuya, G., Liu, F., Hattori, Y., Riechelmann, D.: Asymptotic analysis of radiation extinction of stretched premixed flames. Int. J. Heat Mass Transfer 43(2), 231–239 (2000)
[24] Turns, S.R.: Introduction to Combustion. vol. 287. McGraw-Hill Companies, New York (1996)
[25] Warnatz, J., Maas, U., Dibble, R.W.: Combustion. Springer, Heidelberg (2006)
[26] Bergman, T.L.: Fundamentals of Heat and Mass Transfer. John Wiley & Sons, New York (2011)
[27] Han, W., Chen, Z.: Effects of Soret diffusion on premixed counterflow flames. Combust. Sci. Technol. 187(8), 1195–1207 (2015)
[28] Zeldowitsch, J., Frank-Kamenetzki, D.: A theory of thermal propagation of flame. Dynamics of Curved Fronts, 131–140 (1988)
[29] Law, C.K.: Combustion Physics. Cambridge University Press, Cambridge (2010)
[30] Barenblatt, G., Librovich, V., Makhviladze, G., others.: The Mathematical Theory of Combustion and Explosions. Consultants Bureau (1985)
[31] Law, C., Chao, B.H., Umemura, A.: On closure in activation energy asymptotics of premixed flames. Combust. Sci. Technol. 88(1-2), 59–88 (1993)

[32] Cheatham, S., Matalon, M.: A general asymptotic theory of diffusion flames with application to cellular instability. J. Fluid Mech. 414, 105–144 (2000)
[33] Veeraragavan, A., Cadou, C.P.: Flame speed predictions in planar micro/mesoscale combustors with conjugate heat transfer. Combust. Flame 158(11), 2178–2187 (2011)
[34] Hearn, E.J.: Mechanics of Materials 2: The mechanics of elastic and plastic deformation of solids and structural materials. Elsevier, (1997)
[35] Rosato, D.V., Rosato, D.V.: Plastics engineered product design. Elsevier, Oxford (2003)
[36] von Mises, R.: Mechanik der festen Körper im plastisch-deformablen Zustand. Gott. Nachr. Math. Phys. Klass. 1913, 582–592 (1913)
[37] Bane, S.P.M., Ziegler, J.L., Shepherd, J.E.: Development of one-step chemistry models for flame and ignition simulation. GALCIT Report GALTCITFM. 2010, 53 (2010)
[38] Wang, D., Ji, C., Wang, S., Wang, Z., Yang, J., Zhao, Q: Numerical study on the premixed oxygen-enriched ammonia combustion. Energy Fuels 34(12), 16903–16917 (2020)
[39] Aspden, A., Day, M., Bell, J.: Lewis number effects in distributed flames. Proc. Combust. Inst. 33(1), 1473–1480 (2011)
[40] Sauer, V.M., Dunn-Rankin, D.: Impinging nonpremixed coflow methane–air flames with unity Lewis number. Proc. Combust. Inst. 36(1), 1411–1419 (2017)
[41] Zitouni, S., Brequigny, P., Mounaim-Rousselle, C.: Influence of hydrogen and methane addition in laminar ammonia premixed flame on burning velocity, Lewis number and Markstein length. Combust. Flame 253, 112786 (2023)
[42] Bouvet, N., Halter, F., Chauveau, C., Yoon, Y.: On the effective Lewis number formulations for lean hydrogen/hydrocarbon/air mixtures. Int. J. Hydrogen Energy 38(14), 5949–5960 (2013)
[43] Wang, L.Q., Ge, Y., Ma, H.H.: Revisiting effective Lewis number of combustible mixtures. Fuel. 343, 127909 (2023)
[44] Okafor, E.C., Nagano, Y., Kitagawa, T.: Experimental and theoretical analysis of cellular instability in lean H2-CH4-air flames at elevated pressures. Int. J. Hydrogen Energy 41(15), 6581–6592 (2016)
[45] Bradley, D., Hicks, R.A., Lawes, M., Sheppard, C.G., Woolley, R.: The measurement of laminar burning velocities and Markstein numbers for iso-octane–air and iso-octane–n-heptane–air mixtures at elevated temperatures and pressures in an explosion bomb. Combust. Flame 115(1-2), 126–144 (1998)
[46] Shy, S.S., Liao, Y.C., Chen, Y.R., Huang, S.Y.: Two ignition transition modes at small and large distances between electrodes of a lean primary reference automobile fuel/air mixture at 373 K with Lewis number >> 1. Combust. Flame 225, 340–348 (2021)
[47] Li, Q., Fu, J., Wu, X., Tang, C., Huang, Z.: Laminar flame speeds of DMF/iso-octane-air-N2/CO2 mixtures. Energy Fuels 26(2), 917–925 (2012)
[48] Mott, P., Roland, C.: Limits to Poisson's ratio in isotropic materials. Phys. Rev. B 80(13), 132104 (2009)
[49] Subramanian, S., Sekhar, A.S., Prasad, B.: Influence of combined radial location and growth on the leakage performance of a rotating labyrinth gas turbine seal. J. Mech. Sci. Technol. 29, 2535–2545 (2015)
[50] Tanigawa, Y., Akai, T., Kawamura, R., Oka, N.: Transient heat conduction and thermal stress problems of a nonhomogeneous plate with temperature-dependent material properties. J. Thermal Stresses 19(1), 77–102 (1996)
[51] Göttgens, J., Mauss, F., Peters, N.: Analytic approximations of burning velocities and flame thicknesses of lean hydrogen, methane, ethylene, ethane, acetylene, and propane flames. Symp. (Int.) Combust. 24(1), 129–135 (1992)
[52] Lafay, Y., Renou, B., Cabot, G., Boukhalfa, M.: Experimental and numerical investigation of the effect of H2 enrichment on laminar methane–air flame thickness. Combust. Flame 153(4), 540–561 (2008)
[53] Boyce, M.P.: Gas Turbine Engineering Handbook. Butterworth-Heinemann Inc, Oxford (2011)
[54] Walsh, P.P., Fletcher, P.: Gas Turbine Performance. Wiley, New Jersey (2004)
[55] Gordon, J., Tsuji, H.: Extinction of premixed flames in a stagnation flow considering general Lewis number. Combust. Sci. Technol. 33(1-4), 193–205 (1983)
[56] Vance, F.H., Shoshin, Y., Van Oijen, J.A., de Goey, L.P.H.: Effect of Lewis number on premixed laminar lean-limit flames stabilized on a bluff body. Proc. Combust. Inst. 37(2), 1663–1672 (2019)
[57] Tang, C., Zhang, Y., Huang, Z.: Progress in combustion investigations of hydrogen enriched hydrocarbons. Renew. Sustain. Energy Rev. 30, 195–216 (2014)
[58] Roy, R., Gupta, A.K.: Performance enhancement of swirl-assisted distributed combustion with hydrogen-enriched methane. Appl. Energy 338, 120919 (2023)
[59] Shi, C., Chai, S., Di, L., Ji, C., Ge, Y., Wang, H.: Combined experimental-numerical analysis of hydrogen as a combustion enhancer applied to Wankel engine. Energy 263, 125896 (2023)

How to cite this article: Yu, C., Malayeri, M.M., Böhlke, T., Chen, Z., Minuzzi, F.: Mathematical thermo-mechanical analysis on flame-solid interaction: Steady laminar stagnation flow flame stabilized at a plane wall coupled with thermo-elasticity model. Z Angew Math Mech. e202400554 (2024). https://doi.org/10.1002/zamm.202400554